Ferroelastically controlled ferrovalley states in stacked bilayer systems with inversion symmetry

Yu-Ke Zhang,[1,*] Jun-Ding Zheng [,1,*,†] Wen-Yi Tong [,1,‡] Yi-Feng Zhao [,1] Yi-Fan Tan [,1] Yu-Hao Shen,[1] Zhao Guan,[1] Fang-Yu Yue [,1,3] Ping-Hua Xiang [,1,3] Ni Zhong [,1,3] Jun-Hao Chu,[1,3] and Chun-Gang Duan [1,2,3,§]

[1]*Key Laboratory of Polar Materials and Devices, Ministry of Education, East China Normal University, Shanghai 200241, China*
[2]*Collaborative Innovation Center of Extreme Optics, Shanxi University, Taiyuan, Shanxi 030006, China*
[3]*Shanghai Center of Brain-inspired Intelligent Materials and Devices, East China Normal University, Shanghai 200241, China*

Realizing and manipulating valley polarization is extremely important to valleytronics. Ferrovalley materials with spontaneous valley polarization are excellent candidates for this purpose. However, for intrinsic ferrovalley materials, ferromagnetism or ferroelectric polarization is usually required, limiting the development of valleytronics, as only systems without inversion symmetry are considered. In this paper, using both group theory analysis and band structure calculations, we demonstrate that valley polarization can exist in systems with both time and space inversion symmetry, and the ferroelastic effect can control the ferrovalley states. Choosing stacking bilayer systems as an example, we achieved valley polarization switching using the shear strain, which uncovers the link between ferrovalley and ferroelasticity. Our investigations not only provide a mechanical way to manipulate valley degree of freedom but also enrich the understanding of the coupling between different ferroic properties.

The valley degree of freedom, coded into the momentum space of a two-dimensional (2D) electron system, has attracted intensive attention in recent years. In analogy to charge and spin, it constitutes the binary logic states of crystal electrons, giving rise to promising applications for information storage and processing [1–8]. It is therefore important to achieve spontaneous valley polarization (ferrovalley state, which is a switchable valley state with intrinsic energy difference between opposite valleys) in valley systems for nonvolatile applications. Ferrovalley systems are generally divided into two categories [9–13]. One is the ferromagnetic honeycomb lattice systems in which the time and space symmetry are broken simultaneously, with two inequivalent valley K_+ and K_- points [9,14–18]. The other is the ferroelectric orthogonal lattice systems in which the space inversion symmetry is broken, like the GeSe monolayer, with two inequivalent valley V_x and V_y points [10,19–23]. Furthermore, authors of recent studies have indicated that those mechanisms of spontaneous structure distortion, valley-layer coupling, sliding ferroelectric, and proximity effect can also achieve switchable valley polarization [24–31]. However, all these valley-polarized systems need to break inversion symmetry, which sets a severe limitation on the development of ferrovalley materials and prevents their practical application.

When examining the previous two different ferrovalley systems, we notice that the occurrence of valley polarization is generally accompanied by a symmetry reduction and the

lift of the degeneracy of valleys [9,10]. Taking monolayer GeSe as an example, the point group changes from D_{4h} to C_{2v} when the system transits from paraelectric to ferroelectric phase, and V_x and V_y valleys become energy inequivalent. Surprisingly, we coincidently find that, when uniaxial strain is applied to paraelectric GeSe, which does not break inversion system, valley polarization still appears (see Fig. S2 in the Supplemental Material [32]). We therefore speculate that the key to lifting valley degeneracy is the loss of certain symmetry operations, which connects the equivalent valleys, instead of the existence of inversion center. Consequently, if we can find a system in which the valleys are grouped by no-inversion operations, then we have a chance to reach valley polarization while keeping the system with both time and space inversion symmetry.

Based on the above thoughts, we choose bilayer systems to verify our conjecture. This is because valley systems often exist in layered structures, and operations like twist or sliding can be applied to bilayer systems, providing additional means to change the crystal symmetry [33–39]. Using group theory analysis and electronic structure calculations, we prove that valley polarization can be realized in systems with both time and space inversion. Finally, for such systems, we show that the shear strain can be used to switch valley polarization, which implies the coupling between ferrovalley and ferroelasticity.

We begin with a general analysis of symmetry requirements for valley polarization. Considering a valley system in which certain valleys in the Brillouin zone are connected by certain symmetry operations O_s, their energies are therefore degenerate, and this degeneracy is protected by O_s. If by any means O_s's are all removed, the degeneracy will then be lifted, and valley polarization could occur. Consequently, to
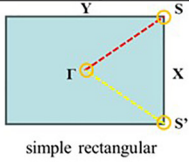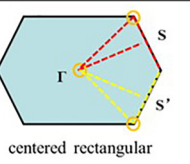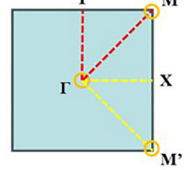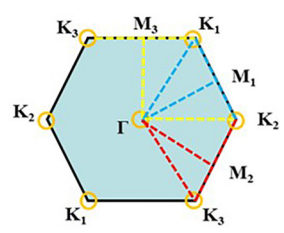
---

*These authors contributed equally to this work.
†jdzheng@phy.ecnu.edu.cn
‡wytong@ee.ecnu.edu.cn
§cgduan@clpm.ecnu.edu.cn

TABLE I. LGs allowing for valley polarization caused by interlayer sliding. In the second column, the different colored dotted lines represent the positions where the polarized valleys can exist. The orange circle indicates that the valleys at that point cannot produce valley polarization. The fourth column is the allowed translation operations, where $G(0, 0)$, $A(\frac{1}{2}, 0)$, $B(0, \frac{1}{2})$, $C(\frac{1}{2}, \frac{1}{2})$, $G'(\frac{1}{4}, \frac{1}{4})$, $A'(\frac{3}{4}, \frac{1}{4})$, $B'(\frac{1}{4}, \frac{3}{4})$, $C'(\frac{3}{4}, \frac{3}{4})$, $G_1(1, 0)$, $M(\frac{1}{3}, \frac{2}{3})$, $N(\frac{2}{3}, \frac{1}{3})$.

Lattice	Brillouin zone	Layer group (Point group)	Translation
Rectangular	simple rectangular / centered rectangular	14-18 (C_{2h})	GA, CB
			General
			G', A', B', C'
		37-48 (D_{2h})	*General*
			G', A', B', C'
Square		51-52 (C_{4h})	A, B
			GB, CA
			GA, CB
		61-64 (D_{4h})	G_1C
			GC
			General
Hexagonal		66 (C_{3i})	A, B, C
			GM, AN
		71 (D_{3d})	GN, BM
			MN
		75 (C_{6h})	GA
			GB
		80 (D_{6h})	GC
			General

achieve valley polarization by any operation, two rules must be obeyed: (i) all the O_s's protecting the degeneracy must be removed simultaneously, and (ii) the new operation should not bring back the degeneracy of valleys.

Following above rules, we then go through 80 layer groups (LGs) for 2D materials [40] to search the candidate LGs that allow valley polarization caused by interlayer sliding operation. The key to the candidate selection is to compare the point groups and specific symmetry operations of the stacking bilayer and monolayer systems after the sliding operations. Through their changes, we can determine whether valley polarization is allowed, as detailed in Sec. 1 in the Supplemental Material [32]. Following the strategy of Ref. [49], we obtain the results of the LGs allowing valley polarization and space inversion symmetry, considering only translation operations (Table I).

To verify the above analysis, we selected the GaBr monolayer as an example, which has good dynamic and thermodynamic stability. The crystal structure of the GaBr monolayer is shown in Fig. 1(a), with the LG and point group $P4/nmm$ (64) and D_{4h}, respectively, which meet the requirements mentioned above. The structural parameters after sufficient relaxation are $a = b = 4.45$ Å, which is marked in Fig. 1(a). Furthermore, we calculated the phonon spectra of the GaBr monolayer. There is no imaginary frequency in phonon spectra shown in Fig. S3 in the Supplemental Material [32], indicating that the GaBr monolayer is dynamically stable. We also calculated the exfoliation energy, and the size is 20.87 meV/Å^2, only slightly larger than MoS$_2$ and graphene

[50]. Figure 1(b) shows the orbital-resolved band structure of the GaBr monolayer. From the band structure, the two equivalent energy valleys (V_x and V_y) are located at X-Γ and Y-Γ paths, which are occupied by p_x and p_y orbitals. Furthermore, based on irreducible representations near the valleys, we can determine that they have linearly polarized light selective absorption, although the energy is degenerate (proofs of the selection rules are provided in Sec. 4 in the Supplemental Material [32]). In general, the symmetry and band structure of GaBr almost perfectly meet the perfect requirements.

Subsequently, we studied the energy of bilayer GaBr with translation operations. As shown in Fig. 1(c), the highest energy is the AA stacking, which corresponds to translation operation $G(0, 0)$. When the upper layer slips 0.5 lattice vectors along the [1,0] or [0,1] direction from AA stacking [translation operation $A(\frac{1}{2}, 0)$ and $B(0, \frac{1}{2})$], the energy of the system reaches its minimum value. Table I shows that these two translation operations allow valley polarization to occur. The two stacking bilayer systems have D_{2h} point group, which are referred to as the V+ and V− states, respectively. Figures 2(d) and 2(e) display the band structures of V+ and V− states, indicating that there is a significant valley polarization; the valley splitting reaches 226.2 meV. We note that the valley splitting mainly occurs in the conduction band, which can be attributed to the stronger electronegativity of Ga atoms. The irreducible representation analysis and optical calculation in Fig. 2(f) shows that valley polarization causes the lift of polarized light absorption at the same time. Eventually, the V+ and V− states appear to x- and y-polarized light
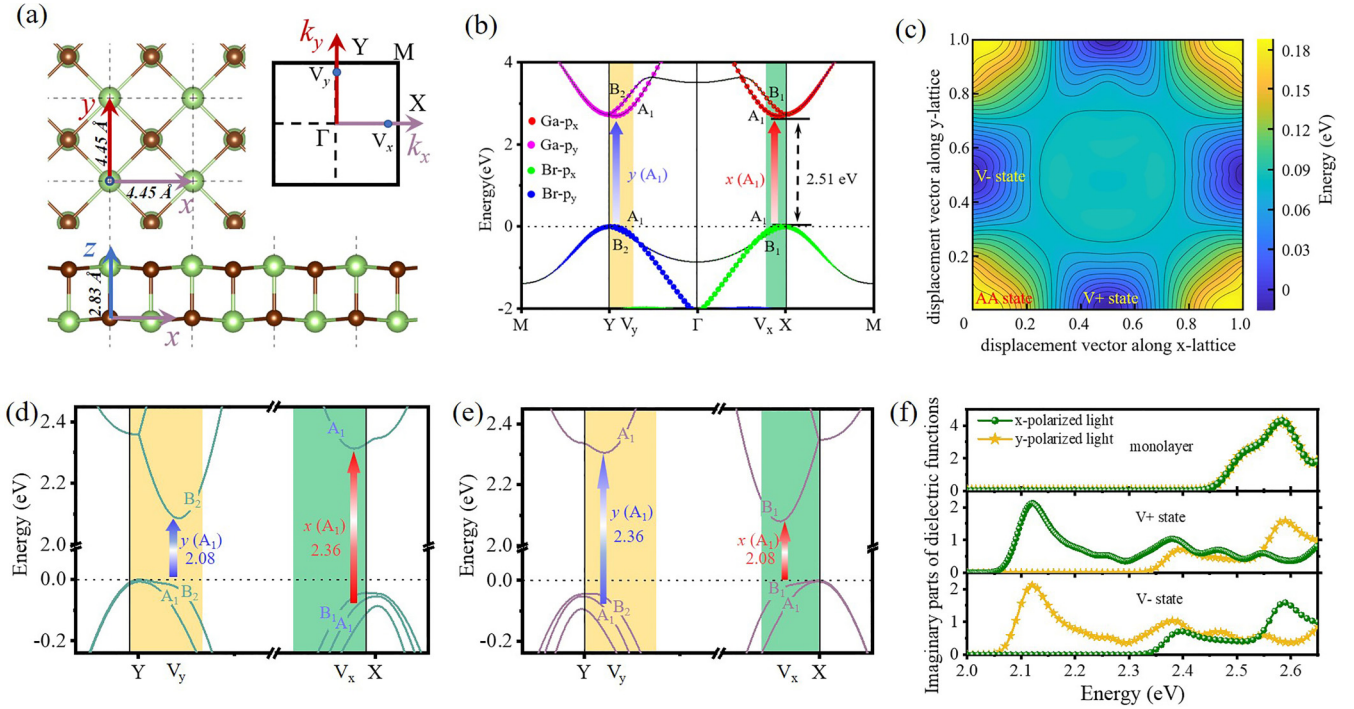
FIG. 1. (a) Crystal structure and (b) orbital-resolved band structure of the GaBr monolayer. (c) Free energy contour for GaBr bilayer vs the displacement of the upper layer. The AA, V+, and V− states are marked. The fine band structure near the valley and the irreducible representation of the conduction band (CB) and valence band (VB) of (d) V+ and (e) V− states. (f) Linear polarization optical absorption of the GaBr monolayer, V+ state, and V− state.

selective absorption, respectively. The existence of optical selective absorption provides a good method for detecting valley polarization.

The relationship between valley polarization and interlayer sliding is analyzed in detail in the square lattice GaBr
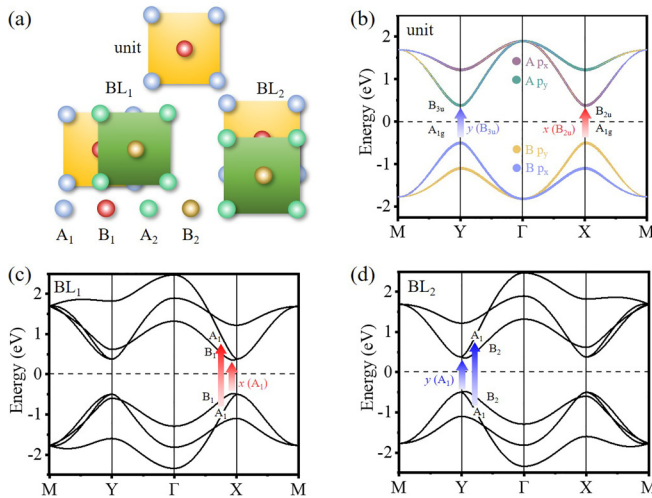

FIG. 2. (a) In the monolayer lattice (unit), m and n atoms are located at the (0.0, 0.0) and (0.5, 0.5) positions of the lattice, respectively. BL$_1$ and BL$_2$ are bilayer structures in which yellow (green) plane denotes the lower (upper) layer. (b)–(d) are band structures of unit, BL$_1$, and BL$_2$, respectively. Red (blue) arrows represent $x(y)$-polarized light. The irreducible representations of the conduction band (CB) and valence band (VB) are marked in (b)–(d).

monolayer. In addition, other 2D Bravais lattices, including rectangular PdAsSe ($P2/b11$, 14), square MoPO$_5$ ($P4/n$, 52), OsTe$_2$ ($P4/mbm$, 63) and hexagonal Bi$_2$Cl$_6$ ($P6/mmm$, 80) [51,52], are simply tested, and they also confirm our conclusion in Fig. S4 in the Supplemental Material [32]. It should be emphasized that the dynamic stability and the allowable sliding position are not discussed; those materials can only serve as a simple verification of our conclusions.

To better understand the physics of valley polarization caused by interlayer sliding, we built a simplified tight-binding (TB) model for a 2D square lattice (D_{4h} point group) with two inequivalent sublattices m and n. Then we consider two different stacking modes (BL$_1$, BL$_2$), both with D_{2h} point group, as shown in Fig. 2(a). The translation operations of BL$_1$ and BL$_2$ are $A(\frac{1}{2}, 0)$ and $B(0, \frac{1}{2})$, and since the GaBr monolayer has two sublayers arranged opposite, which makes BL$_1$ (BL$_2$) correspond to the V− (V+) state in the GaBr monolayer. We describe the band structure of the p-electron system (ignoring the p_z orbital because of its in-plane isotropy) with the above structure [53]. The Hamiltonian of the unit cell in k space $H_{\mathrm{unit}}(k)$ can be written as

$$H_{\mathrm{unit}}(k) = \begin{bmatrix} H^m(k) & H^{mn}(k) \\ \mathrm{H.c.} & H^n(k) \end{bmatrix},$$

$$H^a(k) = M^a I + t_\sigma^a \begin{bmatrix} \cos k_x & 0 \\ 0 & \cos k_y \end{bmatrix}$$
$$+ t_\pi^a \begin{bmatrix} \cos k_y & 0 \\ 0 & \cos k_x \end{bmatrix} (a = m, n),$$
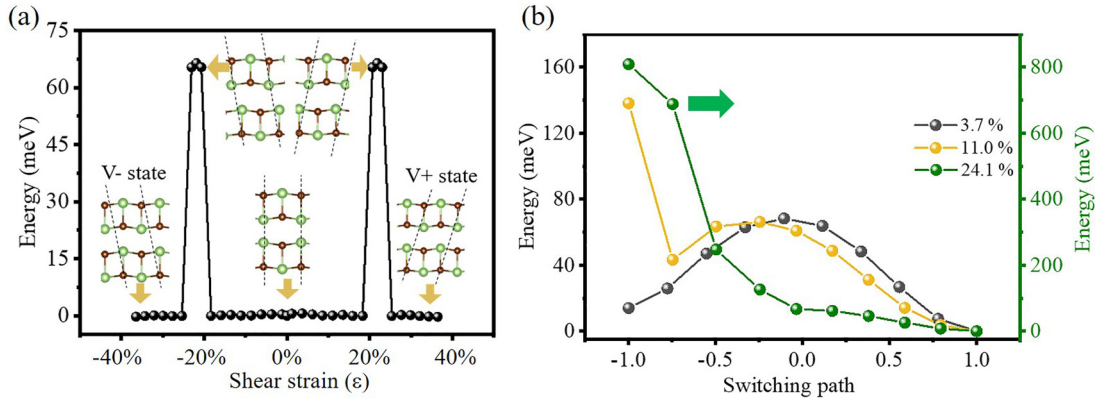
FIG. 3. (a) GaBr bilayer energy vs shear strain [$\varepsilon = \sin^{-1}(\sqrt{-\cos 2\alpha})$]. The energy of the V− state is set as zero, and the structure of relaxation under strain is labeled. (b) The switching barriers under different shear strains calculated by the nudged elastic band method.

$$H^{mn}(k) = t^{mn} \cos\left(\frac{1}{2}k_x\right) \cos\left(\frac{1}{2}k_y\right) I$$
$$+ (-t^{mn}) \sin\left(\frac{1}{2}k_x\right) \sin\left(\frac{1}{2}k_y\right) \sigma_x, \qquad (1)$$

where k is the wave vector, M is the on-site parameter, t is the hopping parameter, σ, π label σ- and π-type bonding, and I and σ_x are the identity matrix and Pauli matrix. With appropriate parameters selected, the orbital-resolved band structure is shown in Fig. 2(b) (see Sec. 3 in the Supplemental Material [32]). There are two valleys with equal energy that exist at X and Y points with p_x- and p_y-orbital occupation, respectively. The irreducible representations at X and Y valleys are also marked in Fig. 2(b), which indicates that there is x (y)-polarized light selective absorption at the X (Y) valley. Overall, the properties of the simplified TB model are very similar to the GaBr monolayer. Next, considering the interlayer nearest-neighbor hopping for BL$_1$, the Hamiltonian $H_{\mathrm{BL}_1}(k)$ can be written as

$$H_{\mathrm{BL}_1}(k) = \begin{bmatrix} H^{11}(k) & H^{12}(k) \\ \mathrm{H.c.} & H^{22}(k) \end{bmatrix}$$
$$H^{12}(k) = \begin{bmatrix} H^{m_1 m_2}(k) & H^{m_1 n_2}(k) \\ H^{n_1 m_2}(k) & H^{n_1 n_2}(k) \end{bmatrix}, \qquad (2)$$
$$H^{a_1 a_2}(k) = \begin{bmatrix} t'^a_\sigma \cos\left(\frac{1}{2}k_x\right) & 0 \\ 0 & 0 \end{bmatrix},$$

where $m_1(n_1)$ and $m_2(n_2)$ represent the $m(n)$ sublattice in the first and second layers. Since there is a large energy difference between m and n sublattices that prevents interlayer orbital hybridization, we ignore $H^{m_1 n_2}$. Then since σ-type bonding is much stronger than π-type bonding, we also ignore t'^a_π in $H^{a_1 a_2}(k)$ (see Sec. 3 in the Supplemental Material [32] for detailed discussion). We can note that the interlayer σ-type bonding of the same sublattices is dominant, which results in strong anisotropy of the interlayer interaction, breaking the C_{4z} and $C_{2,110}$ symmetry operations in the monolayer. Therefore, the degeneracy of Γ-X and Γ-Y is broken, and valley polarization occurs, as shown in Fig. 2(c). On the other hand, the results of irreducible representations show that sliding does not break the selection rule but only changes the optical

band gap. The band structure of BL$_2$ is shown in Fig. 2(d), and its Γ-$X(Y)$ path is equivalent to the Γ-$Y(X)$ path of the BL$_1$ structure due to the different translation operations. In summary, based on the simplified TB model, we obtain similar results to the GaBr bilayer and that the origin of valley polarization can be attributed to the anisotropy interlayer hopping.

Another noteworthy issue is how to achieve valley polarization switching, which is an important feature of a ferrovalley. Due to the presence of inversion symmetry, the valley polarization states cannot be regulated by the electric field, in contrast to sliding ferroelectricity. Interestingly, the relationship between the V+ and V− states is to exchange the x and y axes, which is a ferroelastic phase transition [54,55]. It implies that mechanical strain can switch valley polarization states. We take the V− state as the initial state, applying shear stress by changing the angle between α and β of the crystal and keeping them equal. When $\pm 20\%$ shear strain is applied, the upper and lower atoms show a significant sliding, and the energy increases greatly. Then a transition from the V− to the V+ state occurs. To understand the switching mechanism better, the nudged elastic band calculation method was employed. As shown in Fig. 3(b), the barrier decreases gradually until it disappears completely as the strain increases, indicating that the structure naturally switches from the V− to the V+ state. It is worth noting that 22% strain is a large amount, but experiments have shown that this is an achievable magnitude in some van der Waals materials [56]. We also noticed that the shear strain required to generate sliding in MoS$_2$ and the graphene bilayer is actually much smaller in experiments [57,58]. In fact, the purpose of applying shear strain is to generate atomic displacement to facilitate sliding. During actual operation, applying shear strain in the bilayer system always leads to bending or torsion and promotes atomic displacement, which no longer meets the basic laws of continuum elasticity [59,60]. The result is that a small shear strain is required to cause the interlayer sliding. Although our results may overestimate the shear strain required to switch valley polarization, this does not affect the existence of mechanical stress switching valley polarization.

In summary, we find that the origin of valley polarization is the loss of certain symmetry operations to protect valley degeneracy. Based on this conclusion, we achieve nonvolatile

ferrovalley states that can be switched by shear strain in stacking bilayer systems with inversion symmetry. The general relationship between sliding and valley polarization is analyzed by group theory analysis and is further verified by first-principles and TB model calculations. In addition, we find that valley polarization is coupled with polarized light, which provides a way to experimentally verify valley polarization. Finally, we prove that shear stress realized switching between valley polarization states, which can be regarded as a ferroelastic phase transition. This shows the relationship between valley degrees of freedom and mechanical stress, suggesting the coupling between the ferrovalley and the ferroelastic property. In this paper, we give the general law of valley polarization and significantly expand the ferrovalley family, opening an avenue to explore valley physics.

[1] T. Cao, G. Wang, W. Han, H. Ye, C. Zhu, J. Shi, Q. Niu, P. Tan, E. Wang, B. Liu *et al.*, Valley-selective circular dichroism of monolayer molybdenum disulphide, Nat. Commun. **3**, 887 (2012).

[2] Y. H. Shen, W. Y. Tong, H. Hu, J. D. Zheng, and C. G. Duan, Exotic dielectric behaviors induced by pseudo-spin texture in magnetic twisted bilayer, Chin. Phys. Lett. **38**, 037501 (2021).

[3] Y. Shimazaki, M. Yamamoto, I. V. Borzenets, K. Watanabe, T. Taniguchi, and S. Tarucha, Generation and detection of pure valley current by electrically induced Berry curvature in bilayer graphene, Nat. Phys. **11**, 1032 (2015).

[4] S. A. Vitale, D. Nezich, J. O. Varghese, P. Kim, N. Gedik, P. Jarillo-Herrero, D. Xiao, and M. Rothschild, Valleytronics: Opportunities, challenges, and paths forward, Small **14**, 1801483 (2018).

[5] G. Wang, X. Marie, B. L. Liu, T. Amand, C. Robert, F. Cadiz, P. Renucci, and B. Urbaszek, Control of exciton valley coherence in transition metal dichalcogenide monolayers, Phys. Rev. Lett. **117**, 187401 (2016).

[6] D. Xiao, W. Yao, and Q. Niu, Valley-contrasting physics in graphene: Magnetic moment and topological transport, Phys. Rev. Lett. **99**, 236809 (2007).

[7] W. Yao, D. Xiao, and Q. Niu, Valley-dependent optoelectronics from inversion symmetry breaking, Phys. Rev. B **77**, 235406 (2008).

[8] Z. Ye, D. Sun, and T. F. Heinz, Optical manipulation of valley pseudospin, Nat. Phys. **13**, 26 (2017).

[9] W. Y. Tong, S. J. Gong, X. G. Wan, and C. G. Duan, Concepts of ferrovalley material and anomalous valley Hall effect, Nat. Commun. **7**, 13612 (2016).

[10] X. W. Shen, W. Y. Tong, S. J. Gong, and C. G. Duan, Electrically tunable polarizer based on 2D orthorhombic ferrovalley materials, 2D Mater. **5**, 011001 (2017).

[11] H. X. Cheng, J. Zhou, W. Ji, Y. N. Zhang, and Y. P. Feng, Two-dimensional intrinsic ferrovalley GdI_2 with large valley polarization, Phys. Rev. B **103**, 125121 (2021).

[12] J. Chu, Y. Wang, X. Wang, K. Hu, G. Rao, C. Gong, C. Wu, H. Hong, X. Wang, K. Liu *et al.*, 2D polarized materials: Ferromagnetic, ferrovalley, ferroelectric materials, and related heterostructures, Adv. Mater. **33**, 2004469 (2021).

[13] K. Sheng, Q. Chen, H. K. Yuan, and Z. Y. Wang, Monolayer CeI_2: An intrinsic room-temperature ferrovalley semiconductor, Phys. Rev. B **105**, 075304 (2022).

[14] H. Hu, W. Y. Tong, Y. H. Shen, X. Wan, and C. G. Duan, Concepts of the half-valley-metal and quantum anomalous valley Hall effect, npj Comput. Mater. **6**, 129 (2020).

[15] H. Huan, Y. Xue, B. Zhao, G. Gao, H. Bao, and Z. Yang, Strain-induced half-valley metals and topological phase transitions in MBr_2 monolayers (M = Ru, Os), Phys. Rev. B **104**, 165427 (2021).

[16] P. Jiang, L. L. Kang, Y. L. Li, X. H. Zheng, Z. Zeng, and S. Sanvito, Prediction of the two-dimensional Janus ferrovalley material LaBrI, Phys. Rev. B **104**, 035430 (2021).

[17] C. H. Shen, G. T. Wang, T. X. Wang, C. X. Xia, and J. B. Li, Spin orientation and strain tuning valley polarization with magneto-optic Kerr effects in ferrovalley VS_2 monolayer, Appl. Phys. Lett. **117**, 042406 (2020).

[18] T. Zhang, Y. D. Ma, X. L. Xu, C. G. Lei, B. B. Huang, and Y. Dai, Two-dimensional valleytronics in single-layer t-ZrNY (Y = Cl, Br) predicted from first principles, J. Phys. Chem. C. **124**, 20598 (2020).

[19] C. Chen, X. Chen, Y. Shao, B. Deng, Q. Guo, C. Ma, and F. Xia, Valley-selective linear dichroism in layered tin sulfide, ACS Photonics **5**, 3814 (2018).

[20] K. Jin, E. Oh, R. Stania, F. Liu, and H. W. Yeom, Enhanced Berry curvature dipole and persistent spin texture in the Bi(110) monolayer, Nano Lett. **21**, 9468 (2021).

[21] S. Lin, A. Carvalho, S. Yan, R. Li, S. Kim, A. Rodin, L. Carvalho, E. M. Chan, X. Wang, and A. H. Castro Neto, Accessing valley degree of freedom in bulk tin (II) sulfide at room temperature, Nat. Commun. **9**, 1455 (2018).

[22] J. D. Zheng, Y. F. Zhao, Z. Q. Bao, Y. H. Shen, Z. Guan, N. Zhong, F. Y. Yue, P. H. Xiang, and C. G. Duan, Flexoelectric effect induced *p-n* homojunction in monolayer GeSe, 2D Mater. **9**, 035005 (2022).

[23] A. S. Rodin, L. C. Gomes, A. Carvalho, and A. H. Castro Neto, Valley physics in tin (II) sulfide, Phys. Rev. B **93**, 045431 (2016).

[24] H. Hu, W. Y. Tong, Y. H. Shen, and C. G. Duan, Electrical control of the valley degree of freedom in 2D ferroelectric/antiferromagnetic heterostructures, J. Mater. Chem. C **8**, 8098 (2020).

[25] Y. Wang, W. Wei, F. Li, X. Lv, B. Huang, and Y. Dai, Valley polarization caused by crystalline symmetry breaking, Mater. Horiz. **8**, 244 (2021).

[26] J. Chen, Y. Zhou, J. Yan, J. Liu, L. Xu, J. Wang, T. Wan, Y. He, W. Zhang, and Y. Chai, Room-temperature valley transistors for

low-power neuromorphic computing, Nat. Commun. **13**, 7758 (2022).

[27] Z. M. Yu, S. Guan, X. L. Sheng, W. Gao, and S. A. Yang, Valley-layer coupling: A new design principle for valleytronics, Phys. Rev. Lett. **124**, 037701 (2020).

[28] B. Zhai, R. Cheng, W. Yao, L. Yin, C. Shen, C. Xia, and J. He, Using ferroelectric polarization to regulate and preserve the valley polarization in a $HfN_2/CrI_3/In_2Se_3$ heterotrilayer, Phys. Rev. B **103**, 214114 (2021).

[29] J. D. Zheng, Y. F. Zhao, Y. F. Tan, Z. Guan, N. Zhong, F. Y. Yue, P. H. Xiang, and C. G. Duan, Coupling of ferroelectric and valley properties in 2D materials, J. Appl. Phys. **132**, 120902 (2022).

[30] X. Liu, A. P. Pyatakov, and W. Ren, Magnetoelectric coupling in multiferroic bilayer VS_2, Phys. Rev. Lett. **125**, 247601 (2020).

[31] T. Zhang, X. Xu, B. Huang, Y. Dai, and Y. Ma, 2D spontaneous valley polarization from inversion symmetric single-layer lattices, npj Comput. Mater. **8**, 64 (2022).

[32] See Supplemental Material at http://link.aps.org/supplemental/10.1103/PhysRevB.108.L241120 for details of group theory analysis; details of DFT calculations; details of the TB model and optical selection rule. Supplemental Material also contains Refs. [41–48].

[33] Z. Fei, W. Zhao, T. A. Palomaki, B. Sun, M. K. Miller, Z. Zhao, J. Yan, X. Xu, and D. H. Cobden, Ferroelectric switching of a two-dimensional metal, Nature (London) **560**, 336 (2018).

[34] L. Li and M. Wu, Binary compound bilayer and multilayer with vertical polarizations: Two-dimensional ferroelectrics, multiferroics, and nanogenerators, ACS Nano **11**, 6382 (2017).

[35] X. Liu, Y. Yang, T. Hu, G. Zhao, C. Chen, and W. Ren, Vertical ferroelectric switching by in-plane sliding of two-dimensional bilayer WTe_2, Nanoscale **11**, 18575 (2019).

[36] Q. Yang, M. Wu, and J. Li, Origin of two-dimensional vertical ferroelectricity in WTe_2 bilayer and multilayer, J. Phys. Chem. C **9**, 7160 (2018).

[37] K. Yasuda, X. Wang, K. Watanabe, T. Taniguchi, and P. Jarillo-Herrero, Stacking-engineered ferroelectricity in bilayer boron nitride, Science **372**, 1458 (2021).

[38] D. Yang, J. Wu, B. T. Zhou, J. Liang, T. Ideue, T. Siu, K. M. Awan, K. Watanabe, T. Taniguchi, Y. Iwasa *et al.*, Spontaneous-polarization-induced photovoltaic effect in rhombohedrally stacked MoS_2, Nat. Photon. **16**, 469 (2022).

[39] M. Vizner Stern, Y. Waschitz, W. Cao, I. Nevo, K. Watanabe, T. Taniguchi, E. Sela, M. Urbakh, O. Hod, and M. Ben Shalom, Interfacial ferroelectricity by van der Waals sliding, Science **372**, 1462 (2021).

[40] E. Hitzer and D. Ichikawa, Representation of crystallographic subperiodic groups in Clifford's geometric algebra, Adv. Appl. Clifford Algebras **23**, 887 (2013).

[41] P. E. Blochl, Projector augmented-wave method, Phys. Rev. B **50**, 17953 (1994).

[42] G. Kresse, J. Furthmuller, and J. Hafner, Theory of the crystal structures of selenium and tellurium: The effect of generalized-gradient corrections to the local-density approximation, Phys. Rev. B **50**, 13181 (1994).

[43] G. Kresse and J. Furthmüller, Efficient iterative schemes for *ab initio* total-energy calculations using a plane-wave basis set, Phys. Rev. B **54**, 11169 (1996).

[44] J. P. Perdew, K. Burke, and M. Ernzerhof, Generalized gradient approximation made simple, Phys. Rev. Lett. **77**, 3865 (1996).

[45] G. Kresse and D. Joubert, From ultrasoft pseudopotentials to the projector augmented-wave method, Phys. Rev. B **59**, 1758 (1999).

[46] G. Henkelman, B. P. Uberuaga, and H. Jónsson, A climbing image nudged elastic band method for finding saddle points and minimum energy paths, J. Chem. Phys. **113**, 9901 (2000).

[47] K. Momma and F. Izumi, VESTA: A three-dimensional visualization system for electronic and structural analysis, J. Appl. Crystallogr. **41**, 653 (2008).

[48] A. Togo, First-principles phonon calculations with PHONOPY and PHONO3PY, J. Phys. Soc. Jpn. **92**, 012001 (2022).

[49] J. Ji, G. Yu, C. Xu, and H. J. Xiang, General theory for bilayer stacking ferroelectricity, Phys. Rev. Lett. **130**, 146801 (2023).

[50] J. H. Jung, C.-H. Park, and J. Ihm, A rigorous method of calculating exfoliation energies from first principles, Nano Lett. **18**, 2759 (2018).

[51] S. Haastrup, M. Strange, M. Pandey, T. Deilmann, P. S. Schmidt, N. F. Hinsche, M. N. Gjerding, D. Torelli, P. M. Larsen, A. C. Riis-Jensen *et al.*, The computational 2D materials database: High-throughput modeling and discovery of atomically thin crystals, 2D Mater. **5**, 042002 (2018).

[52] M. N. Gjerding, A. Taghizadeh, A. Rasmussen, S. Ali, F. Bertoldo, T. Deilmann, N. R. Knøsgaard, M. Kruse, A. H. Larsen, S. Manti *et al.*, Recent progress of the computational 2D materials database (C2DB), 2D Mater. **8**, 044002 (2021).

[53] L. Fu, Topological crystalline insulators, Phys. Rev. Lett. **106**, 106802 (2011).

[54] M. Wu and X. C. Zeng, Intrinsic ferroelasticity and/or multiferroicity in two-dimensional phosphorene and phosphorene analogues, Nano Lett. **16**, 3236 (2016).

[55] C. Zhang, Y. Nie, S. Sanvito, and A. Du, First-principles prediction of a room-temperature ferromagnetic Janus VSSe monolayer with piezoelectricity, ferroelasticity, and large valley polarization, Nano Lett. **19**, 1366 (2019).

[56] Y. Hu, L. You, B. Xu, T. Li, S. A. Morris, Y. Li, Y. Zhang, X. Wang, P. S. Lee, H. J. Fan *et al.*, Ferroelastic-switching-driven large shear strain and piezoelectricity in a hybrid ferroelectric, Nat. Mater. **20**, 612 (2021).

[57] Y. Sun, Y. Wang, E. Wang, B. Wang, H. Zhao, Y. Zeng, Q. Zhang, Y. Wu, L. Gu, X. Li *et al.*, Determining the interlayer shearing in twisted bilayer MoS_2 by nanoindentation, Nat. Commun. **13**, 3898 (2022).

[58] J. Liu, C. Zhu, Z. Zhang, Q. Ren, X. Zhang, Y. Zhang, Y. Jin, W. Qiu, H. Wang, J. Zhao *et al.*, Interlayer shear coupling in bilayer graphene, npj 2D Mater. Appl. **6**, 38 (2022).

[59] Y. Shen and H. Wu, Interlayer shear effect on multilayer graphene subjected to bending, Appl. Phys. Lett. **100**, 101909 (2012).

[60] G. Wang, Z. Dai, J. Xiao, S. Feng, C. Weng, L. Liu, Z. Xu, R. Huang, and Z. Zhang, Bending of multilayer van der Waals materials, Phys. Rev. Lett. **123**, 116101 (2019).